

See discussions, stats, and author profiles for this publication at: <https://www.researchgate.net/publication/269993186>

# Development of Ce<sup>3+</sup> /Eu<sup>3+</sup> Dual-Substituted Hydroxyapatite Coating on Surgical Grade Stainless Steel for Improved Antimicrobial and Bioactive Properties

ARTICLE *in* INDUSTRIAL & ENGINEERING CHEMISTRY RESEARCH · DECEMBER 2014

Impact Factor: 2.59 · DOI: 10.1021/ie504387k

---

CITATIONS

3

---

READS

64

## 4 AUTHORS, INCLUDING:



Karthika Arumugam

Periyar University

7 PUBLICATIONS 39 CITATIONS

[SEE PROFILE](#)



Kavitha Louis

Central University of Tamil Nadu

105 PUBLICATIONS 992 CITATIONS

[SEE PROFILE](#)

# Development of Ce<sup>3+</sup>/Eu<sup>3+</sup> Dual-Substituted Hydroxyapatite Coating on Surgical Grade Stainless Steel for Improved Antimicrobial and Bioactive Properties

Dhanaraj Gopi,<sup>\*,†,‡</sup> Saravanan Sathishkumar,<sup>†,‡</sup> Arumugam Karthika,<sup>†</sup> and Louis Kavitha<sup>§</sup>

<sup>†</sup>Department of Chemistry, and <sup>‡</sup>Centre for Nanoscience and Nanotechnology, Periyar University, Salem 636011, India

<sup>§</sup>Department of Physics, School of Basic and Applied Sciences, Central University of Tamilnadu, Thiruvarur 610101, India

## Supporting Information

**ABSTRACT:** The research goal of this experiment is a successful electrodeposition of cerium/europium substituted hydroxyapatite (Ce/Eu-HAP) on borate-passivated 316L stainless steel (SS). The surface characteristics of the resultant coatings were evaluated by Fourier transform infrared spectroscopy, X-ray diffractometry, scanning electron microscopy, and energy dispersive X-ray analysis. The electrochemical characterization of all the coatings was studied in Ringer's solution, in which Ce/Eu-HAP coating exhibited better anticorrosion property than the other developed coatings. The metal ion release from the coatings was studied by inductively coupled plasma atomic emission spectrometry. With regards to antimicrobial activity against *E. coli*, the Ce/Eu-HAP coating exhibited high resistivity compared with the other developed coatings. The resultant coatings exhibited lower cytotoxicity against human osteosarcoma MG63 cells at various incubation days, which evidence the better bioactive nature of the coatings. Thus, the dual-minerals-substituted HAP coating can play a significant role in biomedical applications.

## INTRODUCTION

Stainless steels, in particular, type 316L, are widely employed as medical implants due to their relatively low cost, ease of fabrication, and reasonable chemical stability. However, the surface of stainless steel is prone to release iron (Fe), chromium (Cr), and nickel (Ni) ions in the human body environment,<sup>1,2</sup> where the release of Cr and Ni ions have shown to be powerful allergens and are demonstrated to be carcinogenic.<sup>3</sup> Therefore, the reduction in metal ion release is preferred to avoid the deleterious effect in the normal bone formation caused by the corrosion products. Bioactive ceramic coatings especially hydroxyapatite [Ca<sub>10</sub>(PO<sub>4</sub>)<sub>6</sub>(OH)<sub>2</sub>, HAP] was developed to coat the surface of the implant material. During the past decades, HAP has been the subject of intensive research due to its chemical similarity to the mineral components of bones and tissues in mammals.<sup>4–7</sup> But, the application of HAP possesses several limitations, which include the lack of antimicrobial activity, that challenge its long-term stability and cause implant failures. The lack of antimicrobial activity causes the increased risk of bacterial adherence and colonization of the implants coated with HAP which leads to a second surgery.<sup>8</sup> Hence, the inclusion of a mineral ion with good antimicrobial property into HAP is adopted to ensure the success of the implants coated with HAP.

Moreover, HAP can incorporate a variety of substitutions for Ca<sup>2+</sup> based on the flexibility of apatite structure. The rare earth ions (e.g., Ce, Eu, La, Y, etc.) substitution into HAP has been rarely reported. These minerals substitutions can alter the crystal structure and can change some material properties.<sup>9–13</sup> Lanthanide ions such as the Ce<sup>3+</sup> ion have been used as antimicrobial agent and can play an important role in preventing caries.<sup>14</sup> However, only a few studies have dealt

with Ce-HAP and their antimicrobial properties.<sup>14,15</sup> It can be noted that the higher content of Ce<sup>3+</sup> ions inclusion in HAP may lead to a better antimicrobial effect but it can also increase the cytotoxicity.<sup>15</sup> To minimize the toxicity, secondary material with good bioactivity can be introduced. For this purpose, the Eu<sup>3+</sup> ion, a functional mimic of the Ca<sup>2+</sup> ions that can affect the bone remodeling cycle and are potentially used for the treatment of bone density disorders such as osteoporosis, is introduced into HAP along with Ce<sup>3+</sup>.<sup>16</sup> Also, Webster et al.<sup>9</sup> compared the effects of doping by several trivalent (Bi<sup>3+</sup>, Y<sup>3+</sup>, La<sup>3+</sup>, and In<sup>3+</sup>) and divalent (Mg<sup>2+</sup>, Zn<sup>2+</sup>) cations and found that bone cell adhered and differentiated earlier on HAP doped with trivalent cations compared to divalent cations. The results of reported studies indicate that an increase in valence of doped cations can improve the surface property and biocompatibility of the doped HAP.

However, due to the continuous interaction with the harsh environment, the HAP or substituted HAP on the metallic surface degrades as time progresses and results in the corrosion of metallic alloy.<sup>17</sup> Hence, the surface treatment of metal alloy prior to the coating is essential for preventing metallic corrosion in long-term implant conditions. Gopi et al.<sup>17,18</sup> have previously reported the successful borate passivation on the 316L SS surface and studied the effect of the HAP coating on it by the electrodeposition method. Many research results have supported the fact of double or multisubstituted coatings for biomedical applications recently.<sup>19,20</sup> Several methods for depositing HAP on metallic implant materials have been

**Received:** August 25, 2014

**Accepted:** December 5, 2014

**Published:** December 5, 2014



explored,<sup>21–30</sup> in which the electrodeposition method has a variety of advantages like coating at low temperature, controlled chemical composition, simple setup, and relatively low expense.<sup>31–35</sup> This is the first attempt by the authors to develop a coating of Ce/Eu-HAP on borate passivated stainless steel by electrodeposition, and there are no reports so far.

In our present work, Ce-HAP, Eu-HAP, and Ce/Eu-HAP coatings were successfully developed on borate passivated 316L SS by the electrodeposition method. The influence of Ce<sup>3+</sup> and Eu<sup>3+</sup> incorporation into HAP was investigated by Fourier transform infrared spectroscopy (FT-IR), X-ray diffractometry (XRD), scanning electron microscopy (SEM), and energy dispersive X-ray analysis (EDAX). The *in vitro* corrosion behavior of the resultant coating in Ringer's solution was also evaluated using potentiodynamic cyclic polarization as well as electrochemical impedance spectroscopic techniques. An inductively coupled plasma atomic emission spectrometric (ICP-AES) study was performed to evaluate the metal and mineral ions released from the above said coatings. In addition, the antimicrobial property of the coatings were evaluated against *Staphylococcus aureus* (*S. aureus*) and *Escherichia coli* (*E. coli*) stains, and also the *in vitro* cytotoxicity test was performed using human osteosarcoma (HOS) MG63 cells to estimate the bioactivity of the coatings.

## MATERIALS AND METHODS

**Preparation of 316L SS Specimens.** The 316L SS (procured from Steel Authority of India Ltd., (SAIL), India) having elemental composition (wt %) C-0.0222, Si-0.551, Mn-1.67, P-0.023, S-0.0045, Cr-17.05, Ni-11.65, Mo-2.53, Co-0.136, Cu-0.231, Ti-0.0052, V-0.0783, N-0.0659 and Fe remainder was used as the substrate for the electrodeposition. The 316L SS substrates were cut into dimensions of 10 × 10 × 3 mm<sup>3</sup> and were embedded in epoxy resin leaving area of 1 cm<sup>2</sup> for exposure to the electrolyte. Prior to the deposition process, all the substrates were abraded with silicon carbide sheets from 400 to 1200 grits. After polishing, the 316L SS substrates were thoroughly washed with deionized (DI) water and ultrasonically cleaned in acetone for 10 min, and then used for further studies.

**Preparation of Electrolyte Solution. Batch 1.** First, Ca(NO<sub>3</sub>)<sub>2</sub>·6H<sub>2</sub>O (0.45 M, 0.425 M, and 0.4 M) and Ce(NO<sub>3</sub>)<sub>3</sub>·6H<sub>2</sub>O (0.05 M, 0.075 M and 0.1 M) were dissolved separately in DI water. The (NH<sub>4</sub>)<sub>2</sub>HPO<sub>4</sub> (0.3 M) was dissolved in DI water and the solutions were mixed in the molar ratio of 1.67. The electrolyte was kept in a magnetic stirrer for 2 h and the pH of the electrolyte was adjusted to 4.5 by using NH<sub>4</sub>OH solution. To maintain the uniform concentration of the electrolyte, the magnetic stirring was controlled at a speed of 180 rpm. In this process, the electrolyte was deaerated with N<sub>2</sub> for 30 min. The resultant Ce-HAP solution was used for the further processes.

**Batch 2.** The Ca(NO<sub>3</sub>)<sub>2</sub>·6H<sub>2</sub>O (0.45 M, 0.425 M and 0.4 M) and Eu(NO<sub>3</sub>)<sub>3</sub>·5H<sub>2</sub>O (0.05 M, 0.075 M and 0.1 M) were dissolved in DI water, separately, and the (NH<sub>4</sub>)<sub>2</sub>HPO<sub>4</sub> (0.3 M) was dissolved in DI water. The solutions were mixed to obtain a solution with a molar ratio of 1.67. The other processes are similar to the previous procedure as given in the description of batch 1. The final Eu-HAP solution was used for the coating process.

**Batch 3.** In this batch, a constant concentration of Ce(NO<sub>3</sub>)<sub>2</sub>·6H<sub>2</sub>O (0.1 M) and different concentrations of Eu(NO<sub>3</sub>)<sub>3</sub>·5H<sub>2</sub>O (0.05 M, 0.075 M and 0.1 M) and Ca(NO<sub>3</sub>)<sub>2</sub>·6H<sub>2</sub>O (0.35 M,

0.325 M and 0.3 M) were taken for the deposition and mixed accordingly. Then, the solutions were mixed with 0.3 M (NH<sub>4</sub>)<sub>2</sub>HPO<sub>4</sub> solution. The remaining process is followed as mentioned previously and the resultant electrolyte solution was used for the coating process. The chemicals used for the electrolyte preparation are all analytical grade.

**Surface Passivation on 316L SS.** To enhance the corrosion resistance of the alloy specimens, surface passivation was carried out by a procedure reported previously.<sup>18</sup> In brief, the samples were potentiostatically held in 0.4 M borate buffer solution (pH 9.3) at 640 mV vs saturated calomel electrode (SCE) for 2 h. An anodic potential of 640 mV vs SCE was applied after which the electrode was gently rinsed in DI water and immediately transferred to the analyzing chamber. Electrochemical deposition of Ce-HAP, Eu-HAP, and Ce/Eu-HAP was carried out on these passivated specimens according to the following procedure.

**Electrodeposition of Resultant Coatings.** The resultant solutions of batch I, batch II, and batch III were used as electrolytes for the electrochemical deposition process where the passivated stainless steel specimens served as cathode, platinum acted as anode, and the standard calomel electrode (SCE) acted as the reference electrode. A constant cathodic potential of -1400 mV vs SCE was applied by means of electrochemical workstation (CHI 760C, CH instruments, USA) for the duration of 1 h in the potentiostatic mode. The temperature during the deposition was maintained at 50 °C. After the electrodeposition, the as-coated specimens were gently rinsed in deionized water and further characterized.

**Surface Characterizations of Coatings.** The FT-IR spectra were obtained using a PerkinElmer RX1 FT-IR spectrometer and were recorded in the 4000–400 cm<sup>-1</sup> region with 4 cm<sup>-1</sup> resolution by using KBr pellet technique. The XRD patterns of the as-coated samples were obtained using PANalytical X'Pert PRO diffractometer in the range between 20° ≤ 2θ ≤ 70° with Cu Kα radiation (1.5406 Å).

The surface morphology and actual composition of the as-deposited samples were observed by a high resolution scanning electron microscopy (HRSEM, JSM 840A, JEOL-Japan) equipped with EDAX.

**Electrochemical Characterizations of Resultant Coatings on Passivated 316L SS.** The corrosion performance of Ce-HAP, Eu-HAP, and Ce/Eu-HAP coatings on borate passivated 316L SS was evaluated by potentiodynamic cyclic polarization and electrochemical impedance spectroscopy (EIS) in Ringer's solution (with composition NaCl, 8.6 g·L<sup>-1</sup>; CaCl<sub>2</sub>·2H<sub>2</sub>O, 0.66 g·L<sup>-1</sup>; and KCl, 0.6 g·L<sup>-1</sup>). The pH of the test solution was adjusted to 7.4 and maintained at a temperature of 37 ± 1 °C. All the electrochemical measurements were carried out using the three electrode cell assembly and the CHI 760 electrochemical workstation (USA).

The working and counter electrodes were passivated 316L SS and platinum, respectively whereas, the SCE served as the reference electrode. All the potential values in the text are related to the SCE. During the cyclic polarization studies, the potential was increased in noble direction with a sweep rate of 0.1 mV·s<sup>-1</sup> until the breakdown potential (E<sub>b</sub>) was reached. The sweep direction was reversed until the scan met the passive region. The breakdown or pitting potential was obtained at the potential where there was a monotonic increase in the current density. The repassivation potential (E<sub>pp</sub>) is the potential at which the reverse scan meets the passive region. The electrochemical impedance studies were performed in the

same setup as that of potentiodynamic polarization studies, and the applied ac perturbation signal was about 5 mV within the frequency range  $10^{-2}$  Hz–100 kHz. A record of obtained data was taken using internally available software. Each electrochemical experiment was repeated three times to ensure reproducibility.

**ICP-AES.** The dissolution study of the Ce/Eu-HAP coating was performed by ICP-AES (Thermo Electron IRIS INTREP-ID II XSP DUO, USA). The fresh Ringer's solution was maintained by immersing the coated specimen for 1, 4, and 7 days.

**Antimicrobial Studies.** The two bacterial strains *S. aureus* (ATCC 25923) and *E. coli* (ATCC 25922) were used to study the in vitro antimicrobial properties of the Ce-HAP, Eu-HAP, and Ce/Eu-HAP coatings using agar disc diffusion technique. The inoculums of the microorganisms were prepared from fresh overnight broth cultures (Tryptic soy broth with 0.6% yeast extract) that were incubated at  $37 \pm 1$  °C. The agar disc diffusion test was performed at Muller-Hinton agar. The diffusion technique was carried out by pouring agar into Petri dishes to form 4 mm thick layers and adding dense inoculums of the tested microorganisms in order to obtain semiconfluent growth. Petri plates were left for 10 min to dry in the air, and after that, discs were prepared from Whatman filter paper and immersed into 100 µL of the as-developed coating powders. The discs were placed at equal distance and incubated for 24 h at 37 °C.<sup>20</sup> Antibiotics like Oxacillin (10 µg) and Amikacin (30 µg) were used as positive control for Gram-positive and Gram-negative bacteria. The antimicrobial activity was measured as the zone of inhibition (mm) around the disc.

**In Vitro Cytotoxicity Test.** MG63 osteoblast-like cells from human osteosarcoma (ATCC CRL-1427TM) supplied by National Centre for Cell Sciences (NCCS), Pune, India, were cultured in standard culture medium, Dulbecco's Modified Eagle Medium (DMEM, GIBCO), which consisted of a minimal essential medium, supplemented with 10% fetal bovine serum (FBS), and 1% nonessential amino acids (GIBCO). The medium was renewed every 2 days, and the cultures were maintained in a humidified atmosphere with 5% CO<sub>2</sub>, at 37 ± 1 °C. The confluent osteoblast cultures were detached from the culture flask by incubation with 0.1% trypsin and 0.1% ethylene diamine tetraacetic acid (EDTA) for 5 min. The growth and viability of cells colonizing the samples were evaluated by measuring the mitochondrial dehydrogenase activity using a modified MTT (3-(4,5-dimethyl-2-tiazolyl)-2,5-diphenyl-2H tetrazolium bromide) assay. To determine the cytotoxicity of the resultant coatings at different concentrations, MG63 cells were seeded in 12-well plates at 10<sup>4</sup> cells/mL in a humidified 5% CO<sub>2</sub> atmosphere. After 24 h of incubation, MTT solution in 1 mL of serum-free medium was added and incubated for 4 h at 37 °C in a humidified 5% CO<sub>2</sub> atmosphere. The solution was then removed, dimethyl sulfoxide was added, and the plate was shaken for 15 min before measuring absorbance at 570 nm (the reference value was 690 nm) on an ELISA microplate reader. The % cell viability was calculated with respect to control as follows:<sup>36</sup>

$$\% \text{ cell viability} = \frac{[\text{A}]_{\text{test}}}{[\text{A}]_{\text{control}}} \times 100$$

**Statistical Analysis.** The antibacterial activity and cytotoxicity tests were performed for the resultant coatings in triplicate and repeated three times (mean  $\pm$  SE). Statistical analysis was performed using analysis of variance (ANOVA) with Tukey's

multiple comparison tests (Prism, version 5.0). The difference observed between samples was considered to be significant at  $P < 0.05$ .

## RESULTS AND DISCUSSION

**Functional Group Analysis.** The FT-IR spectra of HAP, Ce-HAP (0.1 M of Ce), Eu-HAP (0.1 M of Eu), and Ce/Eu-HAP (0.1 M of Ce and 0.1 M of Eu) specimens obtained at optimum conditions are shown in Figure 1a-d. In Figure 1b,

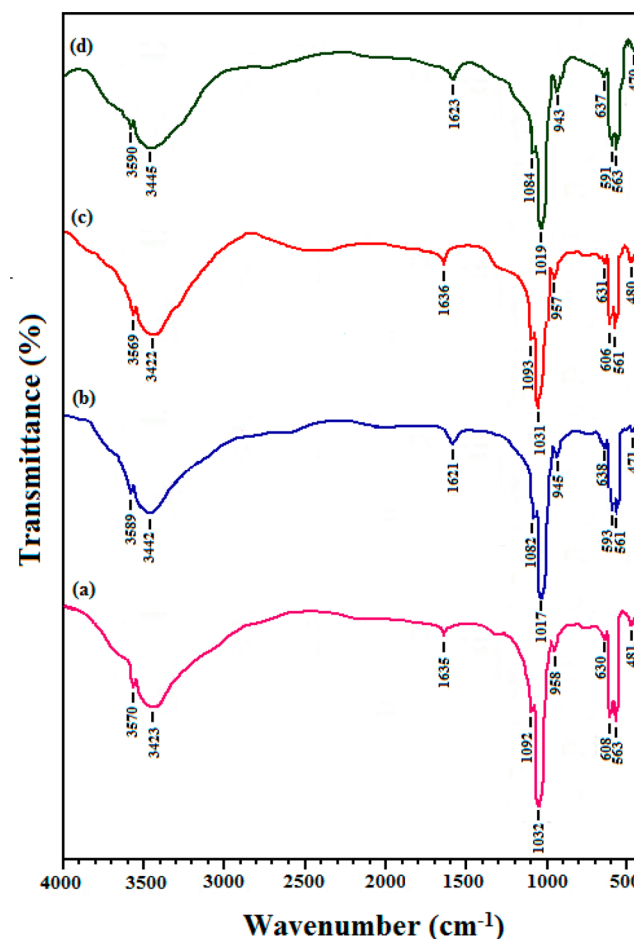


**Figure 1.** FT-IR spectra of (a) HAP, (b) Ce-HAP, (c) Eu-HAP, and (d) Ce/Eu-HAP coatings at optimum conditions.

the characteristic peaks appeared at 1017 and 1082 cm<sup>-1</sup>, 593 and 561 cm<sup>-1</sup>, and 471 cm<sup>-1</sup>, and the band observed at 945 cm<sup>-1</sup> depicts the phosphate groups. The absorption peaks observed at 3589 and 638 cm<sup>-1</sup> are assigned to the stretching and bending vibration of the OH<sup>-</sup> group. In addition, the broad band at 3442 cm<sup>-1</sup> and a peak at 1621 cm<sup>-1</sup> are assigned for the stretching and bending mode of the H<sub>2</sub>O molecule of Ce-HAP, respectively. The FT-IR spectrum of Ce-HAP (Figure 1b) coating shows a similar structure of HAP, but some changes in IR wavenumber of bands are observed due to the substitution of Ca<sup>2+</sup> by Ce<sup>3+</sup> into the apatite lattice where the ionic radius of Ca<sup>2+</sup> is 0.100 nm and Ce<sup>3+</sup> is 0.107 nm. The bigger radius of Ce<sup>3+</sup> consequently decreases the bonding strength of P–O and the OH group. The spectrum (Figure 1c) for Eu-HAP coating contains the bending vibrations of the phosphate groups at 480, 561, and 606 cm<sup>-1</sup>, and their asymmetric stretching vibrations are obtained at 1032 and 1092 cm<sup>-1</sup>. The peaks appearing at

3569 and 631  $\text{cm}^{-1}$  can be attributed to the stretching and librational modes of the  $\text{OH}^-$  ions. In addition, a broad band centered at 3422  $\text{cm}^{-1}$  and a weaker signal at 1636  $\text{cm}^{-1}$  were observed in all the coating samples which correspond to the O-H vibration and the H-O-H bending mode of absorbed water, respectively. From this spectrum, it was observed that the obtained peaks suggested the formation of the HAP phase (Figure 1a); that is, the Eu ion substitution did not influence the HAP phase much, which may be due to the smaller ionic radius of the Eu ion than of the Ca ion.<sup>37</sup> The IR spectrum of the Ce/Eu-HAP coating (Figure 1d) shows a similar structure as that of Ce-HAP. Thus, the FT-IR spectra confirmed the formation of Ce-HAP, Eu-HAP, and Ce/Eu-HAP coatings by the electrodeposition and no other impurities were identified.

**X-ray Diffraction Studies.** The XRD patterns of Ce-HAP (0.1 M of Ce), Eu-HAP (0.1 M of Eu), and Ce/Eu-HAP (0.1 M of Ce and 0.1 M of Eu) are shown in Figure 2a–c. It is

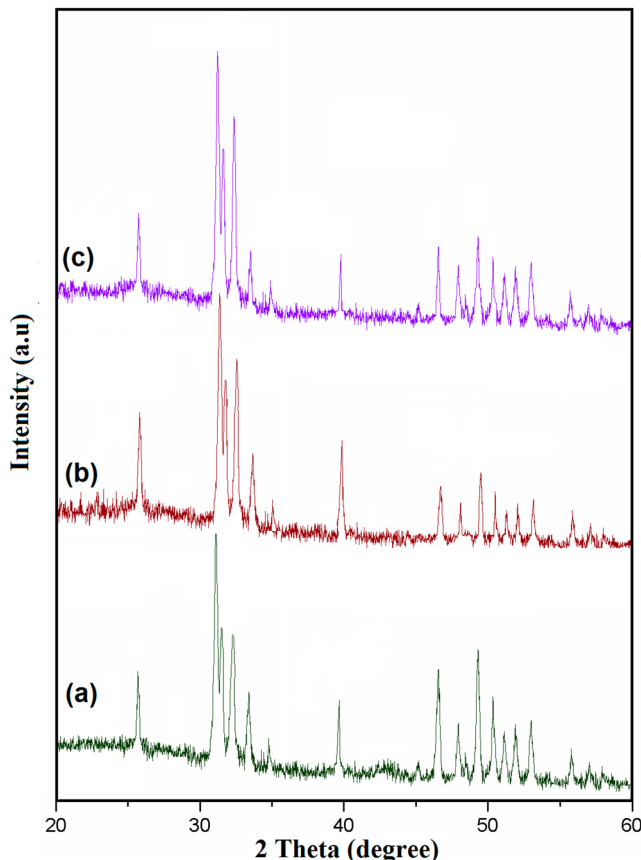


Figure 2. XRD patterns of (a) Ce-HAP, (b) Eu-HAP, and (c) Ce/Eu-HAP coatings at optimum conditions.

obvious that the X-ray diffraction patterns of all coatings agree well with that of the standard data (ICDD No. 09-0432). Figure 2a and c exhibited a slight shift toward the lower diffraction angle which evidence the substitution of the minerals in the HAP lattice. However, Figure 2b showed the diffraction peaks of the HAP-like structure rather than of the Eu-HAP structure. No other impurities can be detected, suggesting the high purity of the obtained coating samples. Moreover, the relative intensities of the diffraction peaks reveal that the as-formed coatings were highly crystalline in nature.

**Morphological Characterization of Resultant Coatings.** The SEM images provide direct information about the typical morphology of the as-coated samples on passivated SS specimens. Figure 3a–c show the SEM images of Ce-HAP

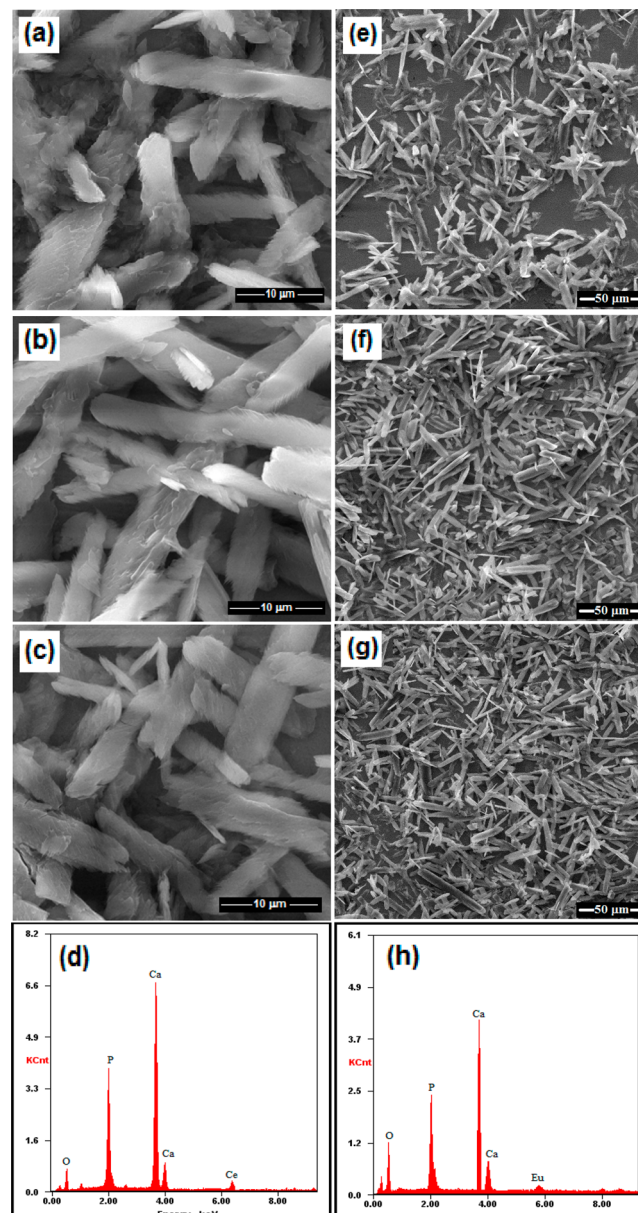
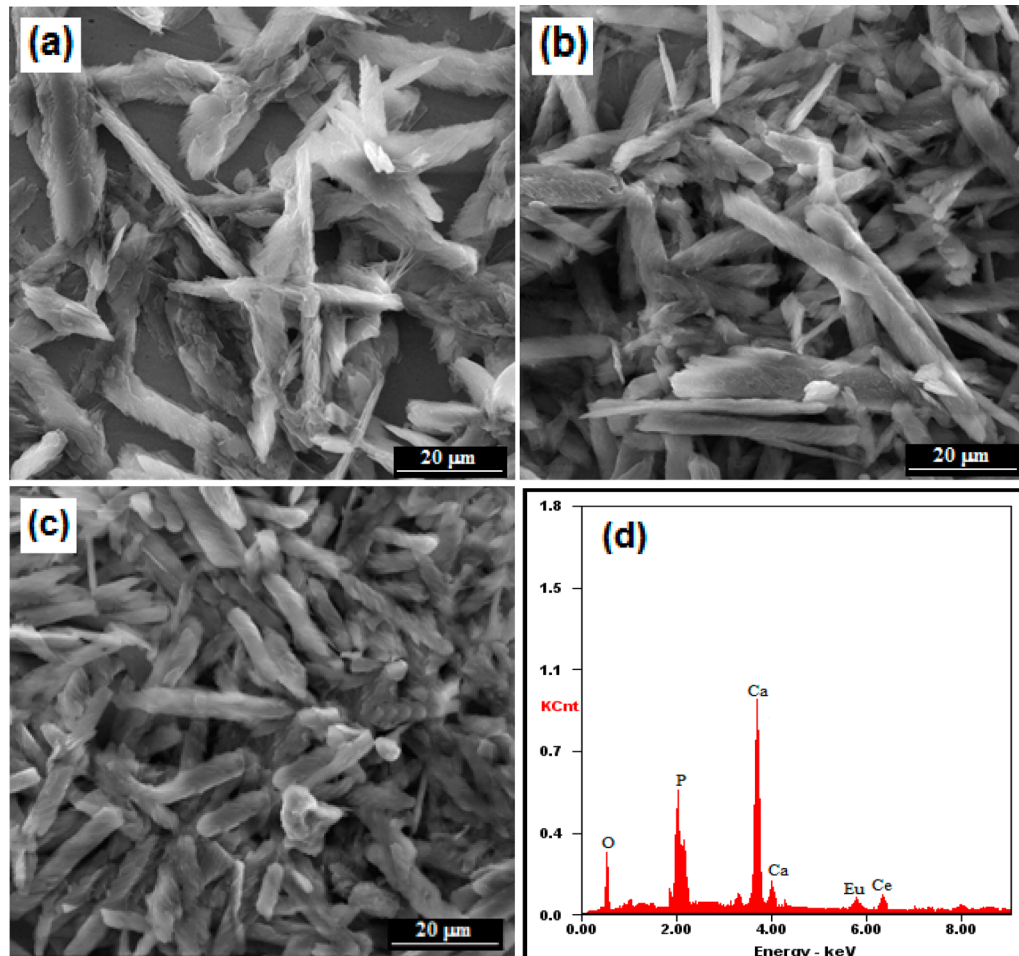


Figure 3. SEM micrographs of (a) Ce-HAP-I, (b) Ce-HAP-II, (c) Ce-HAP-III coatings on passivated 316L SS; (d) EDAX spectrum of the Ce-HAP-III coating; (e) Eu-HAP-I, (f) Eu-HAP-II, (g) Eu-HAP-III coatings on passivated 316L SS; (h) EDAX spectrum of the Eu-HAP-III coating.

coating on passivated 316L SS at different concentrations of  $\text{Ce}^{3+}$  ions, 0.05, 0.075, and 0.1 M, in which Ce-HAP at 0.05 M  $\text{Ce}^{3+}$  (Ce-HAP-I) exhibits the rodlike structure on the passivated SS surface. The structure was not uniform and contained some breakages as shown in Figure 3a. Moreover, the increment of  $\text{Ce}^{3+}$  concentration (0.075 M) in HAP (Ce-HAP-II) produces rods with feather edge morphology (Figure 3b), and the concentration of 0.1 M  $\text{Ce}^{3+}$  in Ce-HAP (Ce-HAP-III) results in a rodlike structure (Figure 3c), which may be due to the influence of higher  $\text{Ce}^{3+}$  ion concentration. Also, Figure 1c



**Figure 4.** Morphological features of (a) Ce/Eu-HAP-I, (b) Ce/Eu-HAP-II, (c) Ce/Eu-HAP-III coatings on passivated 316L SS and (d) EDAX spectrum of the Ce/Eu-HAP-III coating.

displays that the passivated SS was fully covered with rod-shaped Ce-HAP, and the Ce-HAP-III coating was fixed as an optimum condition for  $\text{Ce}^{3+}$  substitution. Figure 3d shows the EDAX spectrum of the Ce-HAP-III coating on the passivated SS, which also establishes the presence of calcium (Ca), phosphorus (P), oxygen (O), and cerium (Ce) on the Ce-HAP-coated surface.

The morphological features of the Eu-HAP coatings on passivated SS at different concentrations of  $\text{Eu}^{3+}$  ions like 0.05, 0.075, and 0.1 M are shown in Figure 3e–g and exhibited a rodlike structure on the passivated 316L SS surface. Upon increasing the concentration of the  $\text{Eu}^{3+}$  ions in HAP (0.1 M), that is, the Eu-HAP-III coating, the sizes of the rods become uniform and the surface of the passivated SS is completely covered with dense rods (Figure 3g), whereas the other concentrations of  $\text{Eu}^{3+}$  in HAP coating (0.05 M (i.e., Eu-HAP-I) and 0.075 M (i.e., Eu-HAP-II)), lack surface coverage (Figure 3e,f), which will result in a poor corrosion performance. So, the Eu-HAP-III coating is established as an optimum condition from the SEM result. The EDAX spectrum (Figure 3h) of Eu-HAP-III coating on passivated SS confirms the presence of Ca, P, O, and Eu in the as-formed coating.

The structural morphologies of the Ce/Eu-HAP coatings on passivated 316L SS obtained at the combination of  $\text{Ce}^{3+}$  and  $\text{Eu}^{3+}$  ions with (I) 0.1 M  $\text{Ce}^{3+}$ , 0.05 M  $\text{Eu}^{3+}$ ; (II) 0.1 M  $\text{Ce}^{3+}$ , 0.075 M  $\text{Eu}^{3+}$ ; and (III) 0.1 M  $\text{Ce}^{3+}$ , 0.1 M  $\text{Eu}^{3+}$  are depicted in

Figure 4a–c. Figure 4a shows the randomly arranged rodlike morphology along with numerous breaks at the end obtained for the Ce/Eu-HAP-I coating, which may be influenced by the high  $\text{Ce}^{3+}$  concentration. Moreover, the surface of the passivated SS was not completely covered by the coating. Similarly, the Ce/Eu-HAP-II coating (Figure 4b) and Ce/Eu-HAP-III coating (Figure 4c) display a rod-structured coating on passivated SS, but Figure 4c exhibits compactly packed and well organized rods on the passivated surface (optimum condition), which may result in good corrosion protection. The EDAX spectrum of Ce/Eu-HAP-III (0.1 M  $\text{Ce}^{3+}$ , 0.1 M  $\text{Eu}^{3+}$ ) on passivated SS confirms the presence of Ca, P, O, Ce, and Eu on the surface of the as-developed sample as shown in Figure 4d.

**Antimicrobial Study of Ce-HAP, Eu-HAP, and Ce/Eu-HAP Coatings.** Usually antimicrobial activities of the samples are tested for the microorganisms that can cause implant related infections.<sup>27</sup> Major infections in the hip and knee joints are caused by the aerobic cocci, most commonly known as *S. aureus* about 23% and coagulase-negative *Staphylococci* about 25%.<sup>31</sup> The as-developed Ce-HAP coating with different concentrations of  $\text{Ce}^{3+}$  (0.05, 0.075, and 0.1 M) was tested for their antimicrobial effect against the pathogenic bacteria *S. aureus* and *E. coli* by the disc diffusion method. The zone of inhibition against both strains for the Ce-HAP coating increases upon increasing the concentration of  $\text{Ce}^{3+}$  ions into the HAP. This is shown in Figure 5. The inhibition zone for the Gram-negative

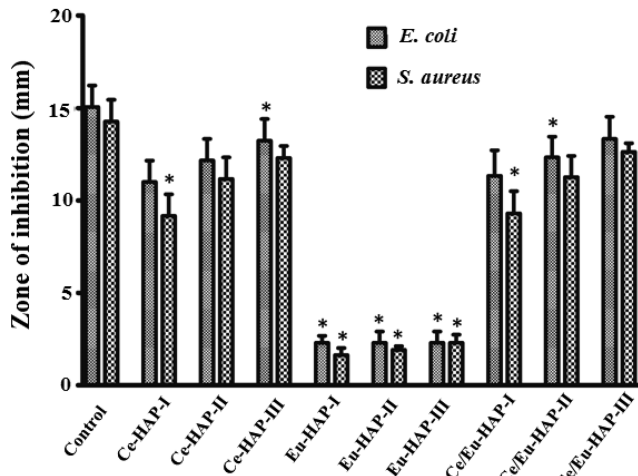


**Figure 5.** A comparison of antimicrobial activities of Ce-HAP, Eu-HAP and Ce/Eu-HAP coatings at different concentrations against pathogenic bacteria *S. aureus* and *E. coli*. The asterisk (\*) denotes a significant difference compared to control ( $P < 0.05$ ).

bacteria, that is, *E. coli*, obtained for the Ce-HAP-III coating was higher than for the increase of the inhibition zone for the Gram-positive bacterial strain (*S. aureus*). Thus, it is clear that the Ce-HAP-III coating exhibits excellent antimicrobial activity and this concentration was taken as an optimum condition for the higher antimicrobial activity.

Also, the Eu-HAP coating developed at various concentrations of Eu (0.05 M, 0.075 M and 0.1 M) was also tested against the bacterial strains *S. aureus* and *E. coli* to examine the antimicrobial activity. In this test, a contrast result was observed for the Eu-HAP coating (as shown in Figure 5), where the Eu-HAP coating shows low protection against the bacteria. The Eu-HAP-I coating exhibits a lower zone of inhibition and the as-formed coating of Eu-HAP-II shows somewhat high inhibition zone. The Eu-HAP-III coating displays much better zone of inhibition than other two coatings. When compared to the bacterial protection with Ce-HAP coating, the Eu-HAP coatings show less protection against the bacteria. Thus, from this study, it clearly shows that the Ce-HAP coating only has the better protection against bacteria.

Also, the dual substituted HAP coating of Ce/Eu-HAP at various concentrations were also tested for antibacterial performances against *S. aureus* and *E. coli*, indicating that the resultant coatings are active against bacteria (Figure 5). The increase of Eu<sup>3+</sup> ion concentration with Ce<sup>3+</sup> in HAP (Ce/Eu-HAP-III) produces the higher inhibition zone which may be due to the higher concentration of Ce<sup>3+</sup> ion as evidenced in Figure 5. This concept was also correlated with the report by Gopi et al.<sup>12</sup> in which Ca-, Sr-, and Ce-substituted HAP exhibited better antimicrobial activity. The zone of inhibition obtained from all the resultant coatings exhibits comparatively less significant values than the control value.

**Cytotoxicity Study of Ce-HAP, Eu-HAP, and Ce/Eu-HAP Coatings.** The cell proliferation of HOS MG63 cells on Ce-HAP and Eu-HAP coatings formed at different concentrations (0.05, 0.075, and 0.1 M) of Ce<sup>3+</sup> and Eu<sup>3+</sup>, respectively, was determined using an MTT assay. The % cell viability on 125 µg/mL of coatings for 1, 4, and 7 days of culture is shown in Figure 6. Owing to the presence of Ce<sup>3+</sup> ions in the Ce-HAP coatings, the cell viability of the coatings was not appreciable while increasing the concentration of Ce<sup>3+</sup> ions and days of

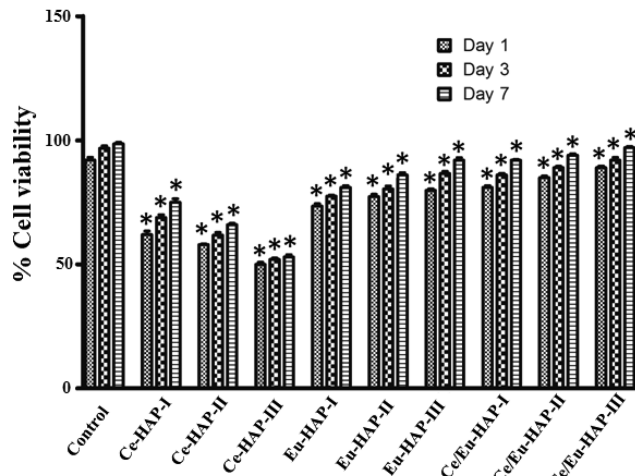


**Figure 6.** *In vitro* cytotoxicity results of Ce-HAP, Eu-HAP, and Ce/Eu-HAP coatings on HOS MG63 cells for 1, 4, and 7 days. The asterisk (\*) denotes a significant difference compared to control ( $P < 0.05$ ).

incubation. Though the Ce-HAP-III coating exhibits high inhibition activity against the bacterial strains, it fails to help the growth of HOS MG63 cells. But, the Eu-HAP coatings obtained with various concentrations exhibit good viability of HOS cells as the concentration of Eu<sup>3+</sup> increases. Also, the viability is found to increase upon increasing the days of culture. The Eu-HAP-II and Eu-HAP-III coatings significantly increased the viability of cells. Cells cultured on Eu-HAP-I coating showed lower cell viability compared to the other coatings. Importantly, the Eu-HAP-II coating exhibits better viability of cells and the coating obtained at 0.1 M of Eu<sup>3+</sup> also showed a similar amount of viability for 7 days incubation, which denotes that both concentrations will produce the same nature of viable character. This clearly evidences that the content of Eu<sup>3+</sup> ions in HAP is a potential for the improvement of biological performance of the coating.

In addition, the cell viability was performed for the as-developed Ce/Eu-HAP coatings at different compositions of Ce<sup>3+</sup> and Eu<sup>3+</sup> ions (Ce/Eu-HAP-I, Ce/Eu-HAP-II, and Ce/Eu-HAP-III) with HOS MG63 cells, and the viability percentages are evaluated by MTT assay (Figure 6). From the MTT assay, it is obvious that the concentration of Eu in Ce/Eu-HAP influenced the cell viability and shows a high percentage of cell growth. From the plot, the viability of MG63 cells on all the coatings is significantly lower as compared to the control. The coated samples with cell lines are observed microscopically for the cell growth or cell damage and compared with control (Figure 7). The as-formed coatings results were compared with cell growth on control as denoted in Figure 7a. The optical image shows that the Ce/Eu-HAP-I are not showing any cell damage, instead it results in cell growth on the coating which demonstrates that the inclusion of Ce<sup>3+</sup> ions has not caused any adverse effect on the coating at 7 days of incubation (Figure 7b). For the Ce/Eu-HAP-II and Ce/Eu-HAP-III coatings, the growth of HOS MG63 cells are appreciable, and there was much difference between them (Figure 7c and d). With the evidence of Figure 6 and Figure 7d, the Ce/Eu-HAP-III exhibits better bioactivity and biocompatibility.

**Potentiodynamic Polarization Studies.** The resistivity of the uncoated 316L SS, Ce-HAP-III, Eu-HAP-III, and Ce/Eu-HAP-III coatings on passivated 316L SS (at optimum

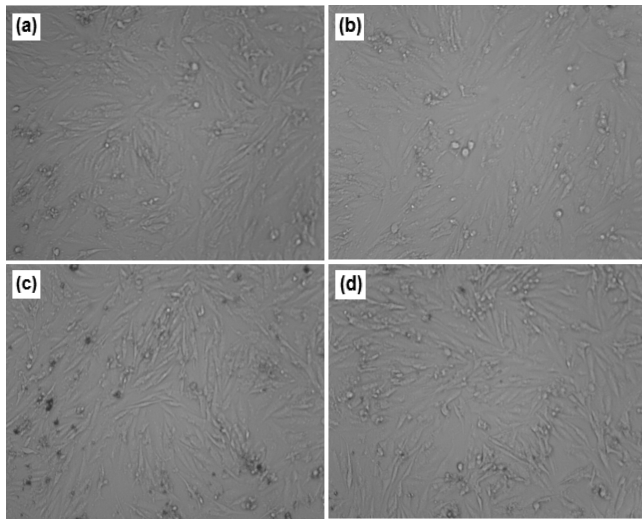


**Figure 7.** Viability images of HOS MG63 cells on (a) control, (b) Ce/Eu-HAP-I, (c) Ce/Eu-HAP-II, and (d) Ce/Eu-HAP-III coating after a cell culture of 7 days.

conditions) in Ringer's solution was assessed by potentiodynamic polarization studies, shown in Supporting Information, Figure S1. The polarization parameters such as corrosion potential ( $E_{corr}$ ), breakdown potential ( $E_b$ ), and repassivation potential ( $E_{pp}$ ) were obtained from the respective polarization plot (Figure S1a). The  $E_{corr}$ ,  $E_b$ , and  $E_{pp}$  values for the uncoated 316L SS specimen were found to be  $-870$  mV,  $+449$  mV, and  $-90$  mV vs SCE, respectively, while the polarization curve recorded for the borate passivated 316L SS specimen was mentioned in our previous report.<sup>18</sup> As seen in the figure, the Eu-HAP coating on the passivated 316L SS specimen has higher  $E_{corr}$ ,  $E_b$ , and  $E_{pp}$  values such as  $-711$  mV,  $+740$  mV, and  $+202$  mV, respectively, than the uncoated pristine 316L SS specimen, which reveals that the coating on passivated SS protects the alloy surface. The Ce-HAP coating on passivated SS possesses  $-650$  mV,  $+783$  mV and  $+247$  mV as  $E_{corr}$ ,  $E_b$ , and  $E_{pp}$  values, respectively, which are higher than that of the Eu-HAP coating. Finally, the polarization curve of the Ce/Eu-HAP coating on passivated 316L SS specimen shows an  $E_{corr}$  value of  $-558$  mV,  $E_b$  value of  $-839$  mV, and  $E_{pp}$  value of  $+268$  mV vs SCE. These  $E_{corr}$ ,  $E_b$ , and  $E_{pp}$  values of the Ce/Eu-HAP coating on passivated 316L SS specimen show a maximum shift in the noble direction when compared to that of the uncoated SS, the Ce-HAP coating, and the Eu-HAP coating on passivated SS specimens. This shift in the  $E_{corr}$ ,  $E_b$ , and  $E_{pp}$  values toward the noble direction is an indication that the Ce/Eu-HAP coating on passivated 316L SS has high corrosion protection in Ringer's solution.

**Electrochemical Impedance Spectroscopic Studies.** Supporting Information, Figure S2 (a–c) shows the Nyquist and Bode plots of the uncoated, Ce-HAP-III, Eu-HAP-III, and

Ce/Eu-HAP-III coatings on passivated 316L SS (at optimum conditions) in Ringer's solution. The acquired polarization resistance ( $R_p$ ) value for the Eu-HAP coating on passivated SS has shown a corrosion resistance  $1600 \Omega \text{ cm}^2$  higher than that obtained for the uncoated 316L SS ( $41 \Omega \text{ cm}^2$ ). For the Ce-HAP coating on passivated SS, the obtained  $R_p$  value is  $2100 \Omega \text{ cm}^2$  which is higher than the uncoated, passivated (reported in ref 18) and Ce-HAP coating on passivated SS. Among all, a highest  $R_p$  value was obtained for the Ce/Eu-HAP coating on passivated 316L SS ( $2349 \Omega \text{ cm}^2$ ), indicating the better and significant corrosion resistance of the coating (Figure S2a). Similarly the Bode plots for the above-mentioned coatings display a maximum total impedance ( $|Z|$ ) value as given in Table 1. The Ce/Eu-HAP coating on passivated 316L SS was found to possess higher  $|Z|$  value ( $2769 \Omega \text{ cm}^2$ ) than those measured for the other specimens as shown in Figure S2b. The Ce-HAP coating on passivated SS and Eu-HAP coating on passivated SS have shown the values as  $2425 \Omega \text{ cm}^2$  and  $1950 \Omega \text{ cm}^2$ , respectively, which are found to be less than that of Ce/Eu-HAP coating. The uncoated SS has shown a low  $|Z|$  value at  $58 \Omega \text{ cm}^2$  when compared with the above coated samples. The Bode phase angle also shows that the Ce/Eu-HAP coating on the passivated SS sample has a high resistivity in Ringer's solution. The phase angle for the Ce-HAP coating and Eu-HAP coating were obtained at a low frequency region and also that of the uncoated SS was attributed to a lesser frequency region than the other coated samples, shown in Figure S2c. Hence the EIS data are in good agreement with the polarization results, and based on the above investigation, it is clear that the Ce/Eu-HAP coating on passivated SS exhibited superior corrosion resistance in physiological solution.

**ICP-AES.** The mineral ions release characteristics of the Ce/Eu-HAP-III coating in Ringer's solution was studied for 1, 4, and 7 days. ICP-AES analysis showed that the release of mineral ions occurred from all the coatings during the first day as shown in Figure 8. The Ca and P ions released in the solution increased at day 1, likewise, the release of Ce and Eu ions in the solution is well evident from Figure 8. Moreover, the mineral ions released for days 4 and 7 are decreased, which may be due to the apatite formation on the coating. Thus, the mineral ions released, such as Ce, Eu, Ca, and P, from the as-developed coatings will be effectively take part in the antibacterial and bioactive properties.

## CONCLUSION

The development of Ce-HAP, Eu-HAP, and Eu/Ce-dual minerals substituted-HAP coatings was successfully achieved on borate passivated 316L SS specimens using the electro-deposition method. The phase purity of the coatings was confirmed by the XRD study and the inclusion of trivalent ions does not influence the phase change of the coatings. We have also investigated the morphological change occurred by varying the content of  $\text{Eu}^{3+}$  and  $\text{Ce}^{3+}$  ions in HAP. The dual minerals

**Table 1.** Electrochemical Parameters of Uncoated SS, Ce-HAP, Eu-HAP, and Ce/Eu-HAP Coatings on Borate Passivated 316L SS

| sample No. | samples                         | $E_{corr}$ (mV) | $E_b$ (mV) | $E_{pp}$ (mV) | $R_p$ ( $\Omega \text{ cm}^2$ ) | $ Z $ ( $\text{cm}^2$ ) |
|------------|---------------------------------|-----------------|------------|---------------|---------------------------------|-------------------------|
| 1          | uncoated pristine 316L SS       | $-870$          | $+449$     | $-90$         | 41                              | 58                      |
| 2          | Eu-HAP on passivated 316L SS    | $-711$          | $+740$     | $+202$        | $1600$                          | $1950$                  |
| 3          | Ce-HAP on passivated 316L SS    | $-650$          | $+783$     | $+247$        | $2100$                          | $2425$                  |
| 4          | Ce/Eu-HAP on passivated 316L SS | $-558$          | $+839$     | $+268$        | $2349$                          | $2769$                  |

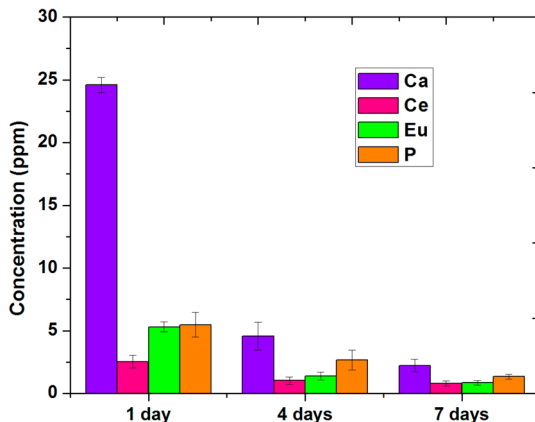


**Figure 8.** ICP-AES analysis of Ce/Eu-HAP coating on passivated 316L SS at different immersion days.

substituted coating (at 0.1 M  $\text{Ce}^{3+}$  and 0.1 M  $\text{Eu}^{3+}$ ) resulted in the uniform coverage on the passivated surface. The dual minerals-substituted coating exhibited appreciable corrosion protection in Ringer's solution than the other coatings. The above results were confirmed through ICP-AES analysis. The antimicrobial activity and cell growth of the dual-substituted HAP coating was excellent and hence proves that the resultant coating can provide better bioactivity and protection against bacteria and hence can be served as better implant material for biomedical applications.

## ASSOCIATED CONTENT

### Supporting Information

Potentiodynamic polarization curves; impedance spectra. This material is available free of charge via the Internet at <http://pubs.acs.org>.

## AUTHOR INFORMATION

### Corresponding Author

\*Tel.: +91 427 2345766. Fax: +91 427 2345124. E-mail: dhanaraj\_gopi@yahoo.com.

### Notes

The authors declare no competing financial interest.

## ACKNOWLEDGMENTS

D. Gopi acknowledges major financial support from the Department of Science and Technology (DST, Reference No. DST/TSG/NTS/2011/73 and Reference No. SB/EMEQ-185/2013) and Council of Scientific and Industrial Research (CSIR, Reference No. 01(2547)/11/EMR-II), New Delhi, India, in the form of major research projects. D. Gopi and L. Kavitha acknowledge the UGC (ref. No. F. 30-1/2013(SA-II)/RA-2012-14-NEW-SC-TAM-3240 and ref. No. F. 30-1/2013(SA-II)/RA-2012-14-NEW-SC-TAM-3228) for the Research Awards. S. Sathishkumar acknowledges the support received from Periyar University in the form of University research fellowship.

## REFERENCES

- (1) Tang, Y.; Katsuma, S.; Fujimoto, S.; Hiromoto, S. Electrochemical study of Type 304 and 316L stainless steels in simulated body fluids and cell cultures. *Acta Biomater.* **2006**, *2*, 709.
- (2) Sivakumar, M.; Rajeswari, S. Investigation of failures in stainless steel orthopaedic implant devices: Pit-induced stress corrosion cracking. *J. Mater. Sci. Lett.* **1992**, *11*, 1039.

(3) Tuken, T. Polypyrrole films on stainless steel. *Surf. Coat. Technol.* **2006**, *200*, 4713.

(4) Song, Y. W.; Shan, D. Y.; Han, E. H. Electrodeposition of hydroxyapatite coating on magnesium alloy for biomaterial applications. *Mater. Lett.* **2008**, *62*, 3276.

(5) Yan, W. Q.; Nakamura, T.; Kawabata, K.; Nishiguchi, S.; Oka, M.; Kokubo, T. Apatite layer-coated titanium for use as bone bonding implants. *Biomaterials* **1997**, *18*, 1185.

(6) Han, Y.; Fu, T.; Lu, J.; Xu, K. Characterization and stability of hydroxyapatite coatings prepared by an electrodeposition and alkaline-treatment process. *J. Biomed. Mater. Res.* **2001**, *54*, 96.

(7) Yang, C.; Yang, P.; Wang, W.; Gai, S.; Wang, J.; Zhang, M.; Lin, J. Synthesis and characterization of Eu-doped hydroxyapatite through a microwave-assisted microemulsion process. *Solid State Sci.* **2009**, *11*, 1923.

(8) Anghelina, F. V.; Ungureanu, D. N.; Bratu, V.; Popescu, I. N.; Rusaneacu, C. O. Fine structure analysis of biocompatible ceramic materials-based hydroxyapatite and metallic biomaterials 316L. *Appl. Surf. Sci.* **2013**, *285*, 65.

(9) Webster, J. T.; Elizabeth, A.; Schuleter, M.; Smith, L. J.; Slomovich, B. E. Osteoblast response to hydroxyapatite doped with divalent and trivalent cations. *Biomaterials* **2004**, *25*, 2111.

(10) Yashukawa, A.; Gotoh, K.; Tanaka, H.; Kandori, K. Preparation and structure of carbonated calcium hydroxyapatite substituted with heavy rare earth ions. *Mater. Res. Bull.* **2012**, *47*, 1257.

(11) Yashukawa, A.; Gotoh, K.; Tanaka, H.; Kandori, K. Preparation and structure of calcium hydroxyapatite substituted with light rare earth ions. *Colloids Surf. A* **2012**, *393*, 53.

(12) Yang, C.; Yang, P.; Wang, W.; Gai, S.; Wang, J.; Zhang, M.; Lin, J. Solvothermal synthesis and characterization of Ln ( $\text{Eu}^{3+}$ ,  $\text{Tb}^{3+}$ ) doped hydroxyapatite. *J. Colloids Interface Sci.* **2008**, *328*, 203.

(13) Joshy, M. I. A.; Elayaraja, K.; Suganthi, R. V.; Veerla, S. C.; Narayana Kalkura, S. In vitro sustained release of amoxicillin from lanthanum hydroxyapatite nano rods. *Curr. Appl. Phys.* **2011**, *11*, 1100.

(14) Yingguang, L.; Zhuoru, Y.; Jiang, C. Preparation, characterization and antimicrobial property of cerium substituted hydroxyapatite nano particles. *J. Rare Earths* **2007**, *25*, 452.

(15) Gopi, D.; Ramya, S.; Rajeswari, D.; Kavitha, L. Strontium, cerium co-substituted hydroxyapatite nanoparticles: Synthesis, characterization, antibacterial activity towards prokaryotic strains and in vitro studies. *Colloids Surf., A* **2014**, *451*, 172.

(16) Chen, F.; Huang, P.; Zhu, Y.; Wu, J.; Zhang, C.; Cui, D. The photoluminescence, drug delivery and imaging properties of multi-functional  $\text{Eu}^{3+}/\text{Gd}^{3+}$  dual-doped hydroxyapatite nanorods. *Biomaterials* **2011**, *32*, 9031.

(17) Gopi, D.; Collins Arun Prakash, V.; Kavitha, L. Evaluation of hydroxyapatite coatings on borate passivated 316L SS in Ringer's solution. *Mater. Sci. Eng., C* **2009**, *29*, 955.

(18) Gopi, D.; Collins Arun Prakash, V.; Kavitha, L.; Kannan, S.; Bhalaji, P. R.; Shinyjoy, E.; Ferreira, J. M. F. A facile electrodeposition of hydroxyapatite onto borate passivated surgical grade stainless steel. *Corros. Sci.* **2011**, *53*, 2328.

(19) Gopi, D.; Ramya, S.; Rajeswari, D.; Surendiran, M.; Kavitha, L. Development of strontium and magnesium substituted porous hydroxyapatite/poly(3,4-ethylenedioxothiophene) coating on surgical-grade stainless steel and its bioactivity on osteoblast cells. *Colloids Surf., B* **2014**, *114*, 234.

(20) Gopi, D.; Karthika, A.; Nithiya, S.; Kavitha, L. In vitro biological performance of minerals substituted hydroxyapatite coating by pulsed electrodeposition method. *Mater. Chem. Phys.* **2014**, *144*, 75.

(21) Gu, Y. W.; Khor, K. A.; Pan, D.; Cheang, P. Activity of plasma sprayed yttria stabilized zirconia reinforced hydroxyapatite/Ti-6Al-4V composite coatings in simulated body fluid. *Biomaterials* **2004**, *25*, 3177.

(22) Zheng, X.; Huang, M.; Ding, C. Bond strength of plasma-sprayed hydroxyapatite/Ti composite coatings. *Biomaterials* **2000**, *21*, 841.

- (23) Liu, D.; Savino, K.; Yates, M. Z. Coating of hydroxyapatite films on metal substrates by seeded hydrothermal deposition. *Surf. Coat. Technol.* **2011**, *20S*, 3975.
- (24) Khandelwal, H.; Singh, G.; Agrawal, K.; Prakash, S.; Agarwal, R. D. Characterization of hydroxyapatite coating by pulse laser deposition technique on stainless steel 316 L by varying laser energy. *Appl. Surf. Sci.* **2013**, *26S*, 30.
- (25) Duta, L.; Oktar, F. N.; Stan, G. E.; Popescu-Pelin, G.; Serban, N.; Luculescu, C.; Mihailescu, I. N. Novel doped hydroxyapatite thin films obtained by pulsed laser deposition. *Appl. Surf. Sci.* **2013**, *26S*, 41.
- (26) Rath, P. C.; Besra, L.; Singh, B. P.; Bhattacharjee, S. Titania/hydroxyapatite bi-layer coating on Ti metal by electrophoretic deposition: Characterization and corrosion studies. *Ceram. Int.* **2012**, *38*, 3209.
- (27) Chew, K.; Zein, S. H. S.; Ahmad, A. L.; McPhail, D. S.; Abdullah, M. F. The electrochemical studies of the corrosion resistance behavior of hydroxyapatite coatings on stainless steel fabricated by electrophoretic deposition. *J. Ind. Eng. Chem.* **2013**, *19*, 1123.
- (28) Han, Y.; Fu, T.; Lu, J.; Xu, K. Characterization and stability of hydroxyapatite coatings prepared by an electrodeposition and alkaline-treatment process. *J. Biomed. Mater. Res.* **2001**, *54*, 96.
- (29) Thanh, D. T. M.; Nam, P. T.; Phuong, N. T.; Que, L. X.; Anh, N. V.; Hoang, T.; Lam, T. D. Controlling the electrodeposition, morphology and structure of hydroxyapatite coating on 316L stainless steel. *Mater. Sci. Eng., C* **2013**, *33*, 2037.
- (30) Gopi, D.; Rajeswari, D.; Ramya, S.; Sekar, M.; Pramod, R.; Jishnu, Dwivedi; Kavitha, L.; Ramaseshan, R. Enhanced corrosion resistance of strontium hydroxyapatite coating on electron beam-treated surgical grade stainless steel. *Appl. Surf. Sci.* **2013**, *286*, 83.
- (31) Bir, F.; Khireddine, H.; Touati, A.; Sidane, D.; Yala, S.; Oudadess, H. Electrochemical depositions of fluorohydroxyapatite doped by Cu<sup>2+</sup>, Zn<sup>2+</sup>, Ag<sup>+</sup> on stainless steel substrates. *Appl. Surf. Sci.* **2012**, *258*, 7021.
- (32) Huang, L. Y.; Xu, K. W.; Lu, J. A study of the process and kinetics of electrochemical deposition and the hydrothermal synthesis of hydroxyapatite coatings. *J. Mater. Sci. Mater. Med.* **2000**, *11*, 667.
- (33) Shirkhanzadeh, M. Bioactive calcium phosphate coatings prepared by electrodeposition. *J. Mater. Sci. Lett.* **1991**, *10*, 1415.
- (34) Manso, M.; Jimenez, C.; Morant, C.; Herrero, P.; Duart, J. M. M. Electrodeposition of hydroxyapatite coatings in basic conditions. *Biomaterials* **2000**, *21*, 1755.
- (35) Gopi, D.; Indira, J.; Kavitha, L. A comparative study on the direct and pulsed current electrodeposition of hydroxyapatite coatings on surgical grade stainless steel. *Surf. Coat. Technol.* **2012**, *206*, 2859.
- (36) Gopi, D.; Shinyjoy, E.; Kavitha, L. Synthesis and spectral characterization of silver/magnesium co-substituted hydroxyapatite for biomedical applications. *Spectrochim. Acta Part A* **2014**, *127*, 286.
- (37) Long, M.; Hong, F.; Li, W.; Li, F.; Zhao, H.; Lv, Y.; Li, H.; Hu, F.; Sun, L.; Yan, C.; Wei, Z. Size-dependent microstructure and europium site preference influence fluorescent properties of Eu<sup>3+</sup>-doped Ca<sub>10</sub>(PO<sub>4</sub>)<sub>6</sub>(OH)<sub>2</sub> nanocrystal. *J. Lumin.* **2008**, *128*, 428.